J|A|C|S
ARTICLES
Published on Web 12/14/2004

Ice Surface Reconstruction as Antifreeze Protein-Induced Morphological Modification Mechanism

Christina S. Strom,[†] Xiang Yang Liu,*[,†] and Zongchao Jia[‡]

Contribution from the Biophysics and Micro/nanostructures Laboratory, Department of Physics, Faculty of Science, National University of Singapore, 2 Science Drive 3, Singapore 117542, and Department of Biochemistry, Queen's University, Kingston, Ontario, Canada K7L 3N6

Received April 23, 2004; E-mail: phyliuxy@nus.edu.sg

Abstract: The crystal growth process by which fish antifreeze proteins (AFPs) and antifreeze glycoproteins (AFGPs) modify the ice morphology is analyzed in the AFP−ice system. A newly identified AFP-induced surface reconstruction mechanism enables one-dimensional helical and irregular globular ice binding surfaces to stabilize secondary, kinetically less stable ice surfaces with variable face indices. Not only are the relative growth rates controlled by the IBS engagement but also the secondary face indices themselves become adjusted in the process of maximizing the AFP−substrate interaction, through attaining the best structural match. The theoretical formulation leads to comprehensive agreement with experiment.

1. Introduction

The antifreeze proteins have evolved to meet the special task of protecting small water and land animals, as well as some plants, from freezing. Their special mode of interaction with the ice lattice suppresses the freezing point of water by up to several degrees. Freezing is a process of ice crystallization from supercooled water. Ice should first experience ice nucleation, followed by growth. Whether or not freezing takes place is determined to a large extent by ice nucleation.[1,2] There is evidence that fish antifreeze proteins bind to and reduce the efficiency of heterogeneous nucleation sites, rather than binding to embryonic ice nuclei.[1,2] Similar phenomena were obtained and explained in refs 3−5. The antifreeze action of the AFP is actually first to inhibit the nucleation by terminating the relevant kinetics.[3−5] When the inhibition of ice nucleation fails, the AFP proceeds to inhibit the growth of ice.

At present, AFP-related research focuses on the detailed action of the AFP on the ice substrates, in the context of either the isolated AFP−ice system or some approximate AFP−ice−water system. In the latter case molecular dynamics (MD) simulations are used to study the equilibrium molecular distribution on the simulated faces. These studies do not deliver a full picture on the AFP-induced morphological modifications of ice crystals for several reasons.

First, in previous AFP studies the morphologically pivotal processes, that is, growth rather than equilibrium processes, have hardly received any attention. In studying the morphology or the morphological modification, one is forced to deal with the mechanisms producing or modifying the face orientations, the surface molecular compositions, as well as the relative growth rates. Examples are the formation of kinks and steps (if the faces are essentially flat) on the ice crystals, the motion of steps, and the transport of impurities and heat. If the AFP is involved, the adsorption of the AFP on the ice surface and the impact of the kink and step integration kinetics should be included. These are not equilibrium but growth mechanisms.

Second, previous studies have not appreciated the crucial distinction between, on one hand, kinetically stable surfaces growing slowly with well-defined unique orientations and, on the other hand, kinetically less stable or unstable surfaces lacking a two-dimensional nucleation barrier and either growing too fast to feature in the morphology or growing as roughened faces. Only the so-called "primary" surfaces, which are limited in number, have the capacity to grow slowly, maintaining a well-defined surface orientation and assuming a flat appearance; other surfaces do not have that capacity.[7]

In dealing with the adsorption of the AFP on specific ice surfaces,[6,8,9] previous studies suffer from a common drawback: the ice substrates[6,10,11] considered available for the AFP action are produced by cutting randomly the hexagonal ice structure and juxtaposing the AFP ice binding surface to those planar cut substrates, without calling to question the crystallographic validity of the randomly obtained planar cut surfaces. In some cases[10,11,25] surfaces were used that are either kinetically totally unstable or molecularly roughened and in either case are incapable of layer growth. Crystallographically valid surfaces

[†] National University of Singapore.
[‡] Queen's University.

(1) Jia, Z.; DeLuca, C. I.; Chao, H.; Davies, P. L. *Nature* **1996**, *384*, 285−288.
(2) Wilson, P. W.; Leader, J. P. *Biophys. J.* **1995**, *68*, 2098−2107.
(3) Du, N.; Liu, X. Y. *Appl. Phys. Lett.* **2002**, *81*, 445−447.
(4) Du, N.; Liu, X. Y.; Hew, C. L. *J. Biol. Chem.* **2003**, *278*, 36000−36004.
(5) Liu, X. Y.; Du, N. *J. Biol. Chem.* **2004**, *279*, 6124−6131.
(6) Jia, Z.; Davies, P. L. *Trends Biochem. Sci.* **2002**, *27* (2), 101−106 and references therein.
(7) Strom, C. S.; Liu, X. Y.; Jia, Z. *J. Biol. Chem.* **2004**, *279*, 32407−32417.
(8) Antson, A. A.; Smith, D. J.; Roper, D. I.; Lewis, S.; Caves, L. S. D.; Verma, C. S.; Buckley, S. L.; Lillford, P. J.; Hubbard, R. E. *J. Mol. Biol.* **2001**, *305*, 875−889.
(9) Knight, C. A. *Crystal Growth Des.* **2001**, *14*, 429−438.
(10) Dalal, P.; Sonnichsen, F. D. *J. Chem. Inf. Comput. Sci.* **2000**, *40*, 1276−1284.
(11) http://pout.cwru.edu/~frank/afp1/.

10.1021/ja047652y CCC: $30.25

satisfy strict conditions, not one of which is the need to be planar cut slices of the structure. On the contrary, they can be bounded by heavily undulating and corrugated surface boundaries.[14,16,18] Both the AFP−ice interaction and the molecular equilibrium distribution in the AFP−ice−water system depend on the detailed definition of the simulated ice crystal substrates. Whenever those substrates are invalid, so are the obtained results.

Third, the appearance of some pyramidal forms on ice crystals grown under the influence of the AFP has thus far been based on the incorrect assumption that crystallographic face orientations could be averaged. The pyramid has been explained[1,19] as the occurrence of an intermediate orientation between the basal face and the primary prism. For example, it is held in ref 1 that reduction of the (100) prismatic growth rate could give rise to a pyramid; it is also held in ref 19 that the (201) pyramid could result from some sort of intersection between the basal face and the primary prism when the RD3 AFP attaches one terminus of its IBS on the basal face (001) and the other terminus on the prism (100). In reality, given two adjacent primary surfaces, two possible occurrences can take place: either one of these will suppress the other if its growth rate is dominantly lower or both will appear on the crystal, their relative importance being reflected in their relative growth rates. However, some intermediate surface, which by the above definition is not a valid primary surface, being adjacent to both of the above primary surfaces, will never appear on the crystal as a "crystallographic average" between the two original faces, regardless of their respective growth rates. The commonly observed phenomenon of surface roughening that gives crystals a rounded appearance has likely been confused with the erroneous assumption of crystallographic averaging.

Fourth, the exceptional morphological occurrence of variable face orientations in AFP-modified ice has escaped attention. One of the most striking characteristics of the ice crystallites produced by fish AFPs and AFGPs is the large variety of secondary prismatic and especially pyramidal forms observed.[20] These shapes correlate directly to specific mutant AFP variants and indirectly to the experimental conditions. This is in sharp contrast to the constant and consistently predictable facet orientations, usually (001) and (100), associated with the ice crystal morphology triggered by the insect AFPs.[7] Since one may not expect the variation in pyramidal shapes to result from a variation in the lattice constants, that variation must be based on a strong variation of the pyramidal face indices.

The ice binding surface (IBS) of insect AFPs is two-dimensional, rigid, planar, and repetitive with regularly spaced binding intervals.[44,45] The IBS of fish AFPs and AFGPs has binding sites that either are one-dimensional with regularly and linearly arranged biding intervals or are two-dimensional but lack a regular arrangement of binding sites.[41] Experimentally, the former correlates with the kinetically stable primary ice surfaces having unambiguous orientations while the latter correlates with the kinetically less stable secondary surfaces having adjustable orientations. The periodic bond chain (PBC) theory of Hartman and Perdok[12−18] enables us to explain the experimentally observed indices of the ice facets and identify the mechanism causing their morphological modification. The theory considers the AFP action on the bare ice substrates to be the major external factor affecting the morphology. This work shows that the fish-type IBS acts to adjust the orientations and stabilize kinetically less stable secondary ice surfaces through the morphological modification mechanism of surface reconstruction.

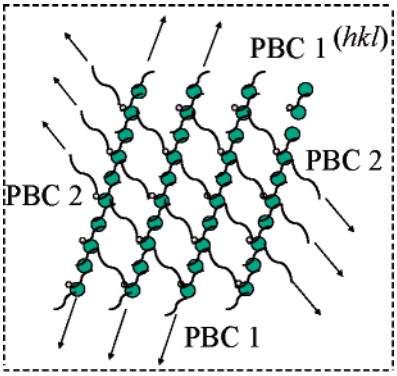

Figure 1. Schematic illustration of a primary, kinetically stable surface drawn face-on. Its molecular composition consists of intersecting PBC1 and PBC2, both parallel to (*hkl*), as outlined by dotted lines. Growth units (molecules) are related by lattice translations parallel to the growing surface (conforming to the "flatness"condition).

2. PBC Theory

The occurrence of crystallographic faces on a crystal cannot be arbitrary; it is controlled by the growth kinetics of specific faces. Crystal surface properties can be analyzed quantitatively by the periodic bond chain (PBC) theory developed by Hartman and Perdok (cf. some original references[12−17] and an extensive list of references[18]). The growth of a primary surface is governed by two-dimensional nucleation or spiral growth, due to the nonzero step free energy in two nonparallel crystallographic directions; hence growth proceeds in a layer-by-layer manner.

A PBC is an uninterrupted chain (or bundle of chains) of strong bonds and has a well-defined crystallographic direction [*uvw*]. Strong bonds are bonds between growth units (usually molecules) in the first coordination sphere. The PBC molecular composition is (a fraction of) the unit cell, and it may not contain lattice translations diverging from [*uvw*]. A PBC is actually a family of infinitely many parallel identical chains, differing only by lattice translations.[14,16,18] A primary surface, illustrated in Figure 1, is parallel to (at least two) intersecting PBCs,[14,16,18] so it has a fixed surface orientation given by $(hkl) = [uvw]_1 \times [uvw]_2$, where $[uvw]_1$ and $[uvw]_2$ are PBC directions. The layer-by-layer growth mechanism is attributed to the two-dimensional network of strong bonds in (*hkl*) formed by the intersecting PBCs. The growth layer is generated by repeated lattice translations along (*hkl*) of a basic block equivalent to the unit cell and has thickness d_{hkl}.

An essential property is the crystallographic condition of "flatness",[14,16,18] responsible for layer growth and the emergence

(12) Hartman, P.; Perdok, W. G. *Acta Crystallogr.* **1955**, *8*, 49, 521.
(13) (a) Hartman, P. *Acta Crystallogr.* **1956**, *9*, 569−572 and 721−727. (b) Hartman, P. *Acta Crystallogr.* **1958**, *11*, 365−369 and 459−464.
(14) Hartman, P. The dependence of crystal morphology on crystal structure. In *Growth of Crystals*; Sheftal, N. N., Ed.; Consultants Bureau: New York, 1969; Vol. 7, pp 3−18.
(15) Hartman, P. Crystal Growth. An Introduction. In *Crystal Growth*; Hartman, P., Ed.; North-Holland: Amsterdam, 1973; pp 367−401.
(16) (a) Strom, C. S. *Z. Kristallogr.* **1980**, *153*, 99. (b) Strom, C. S. *Z. Kristallogr.* **1981**, *154*, 31. (c) Strom, C. S. *Z. Kristallogr.* **1985**, *172*, 11.
(17) Strom, C. S.; Hartman, P. *Acta Crystallogr. A* **1989**, *45*, 371−380.
(18) Strom, C. S. Ionic Crystals. Chapter 5 in *Molecular Modeling Applications in Crystallization*; Myerson, A. S., Ed.; Cambridge University Press: New York, 1999; pp 228−312 and references therein.
(19) Miura, K. *J. Biol. Chem.* **2001**, *276* (2), 1304−1310.
(20) Zhang, W.; Laursen, R. A. *FEBS Lett.* **1999**, *430*, 372−376.

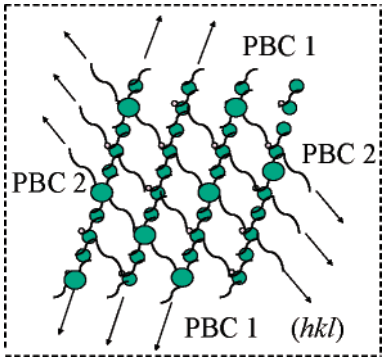

Figure 2. Schematic illustration of a flatness-violating, molecularly roughened surface, drawn face-on. Even though its molecular composition consists of two intersecting PBCs, the growth units (molecules) are related by lattice translations oblique to the growing surface (larger units are above the face, differing by lattice translations from the smaller growth units that are below the face). For that reason the depicted surface configuration is crystallographically invalid.

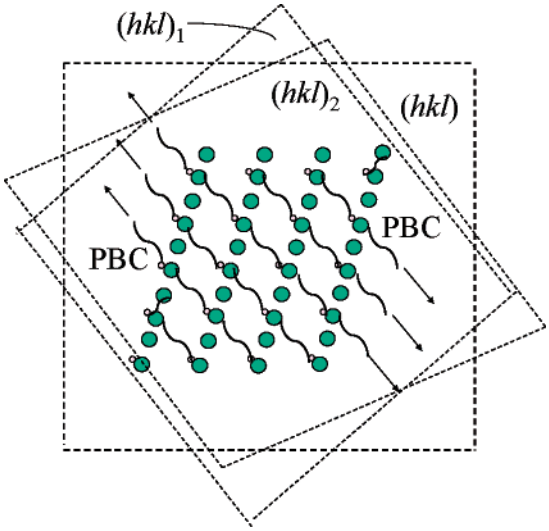

Figure 3. Schematic illustration of a secondary surface that is structurally capable of becoming stabilized, drawn face-on. Its molecular composition consists of only one PBC. Now infinitely many faces (*hkl*), $(hkl)_1$, $(hkl)_2$, etc., outlined by dotted lines are parallel to the single PBC direction, making the surface orientation indeterminate.

of flat surfaces in crystals: the basic block generating the growth layer should not contain lattice translations oblique to the growth front. Its violation results in roughened growth, according to which growth units are deposited in subsequent layers before the underlying layers can be completed. Because the lattice translations in such surfaces, illustrated schematically in Figure 2, are not restricted to be parallel to the face, crystal growth is not restricted to lateral, face-parallel directions. Such surfaces cannot follow a strict layer-by-layer growth mechanism. Interlayer growth becomes possible and inevitable. The surface grows randomly away from the face. Roughened growth is the result.

Surfaces possessing only one strong-bonding direction, the so-called secondary surfaces, lack a two-dimensional nucleation barrier, and deviations from that face parallel to the strong-bonding direction cannot be suppressed. Such a surface, illustrated schematically in Figure 3, experiences accelerated growth and will soon disappear from the growth form, even if it did occur at the beginning. (Obviously the above holds also for a surface possessing no strong-bonding directions at all, hence being kinetically totally unstable; it should be left out of consideration.) Because infinitely many faces exist parallel to any given single strong-bonding direction, the orientation of a secondary surface possessing only one strong-bonding direction is indeterminate, meaning that its face indices are variable. Such surfaces are less stable but may grow by a layer mechanism under exceptional circumstances.

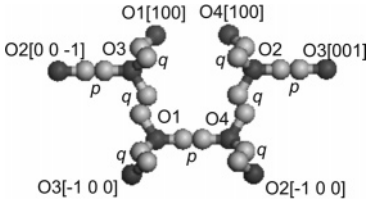

Figure 4. Unit cell of hexagonal ice consisting of water molecules with oxygen atoms 1−4, projected on a plane perpendicular to the *b*-axis, and for each oxygen the strong bonds (*p*, *q*, *q*, *q*) in the first coordination sphere. Each strong bond consists of two O−O links, mediated by two hydrogen atoms. Dark balls, oxygen atoms; light balls, hydrogen atoms.

Table 1. Fractional Axial Coordinates *x*, *y*, and *z* of the Positions of the Four Oxygen Atoms in the Unit Cell of Ice

	x	y	z
O1	0.3333	0.6667	0.0622
O2	0.6667	0.3333	0.5622
O3	0.6667	0.3333	−0.0622
O4	0.3333	0.6667	0.4378

The observed crystal morphology is a composite effect of a basic or structural morphology, for which the structure is responsible, often subjected to a morphological modification effect due to external factors. The structural morphology can be derived[14,16,18] from the primary surfaces. The higher the slice energy (that is, the amount of energy contained in that growth layer), or equivalently the lower the attachment energy (that is, the amount of energy released when a new growth layer becomes attached to the crystal), the lower the growth rate and the more important the face.[14,18] The optimal molecular composition of a primary surface is the one with the lowest attachment energy.[14,16,18] It is empirically found that the growth rates are proportional to the attachment energies. Whether or not a primary surface will actually appear on the growth form, and to what extent it will dominate the morphology, depends on the relative growth rates of the neighboring surfaces. The morphological modification caused by external factors can be assessed from knowledge of the growth conditions, that is, usually the surrounding liquid, often containing influential molecular species. Such species may exert an even stronger morphological effect than the liquid itself, as is the case with the AFP.

3. PBC Analysis of Hexagonal Ice

Figure 4 shows the O atoms in the unit cell and their respective strong bonds. Hexagonal ice belongs to the space group $P6_3/mmc$, $a = 4.519$ Å and $c = 7.357$ Å. The unit cell contains four water molecules, taken at the oxygen positions (cf. Table 1). The O−O bonds, having lengths $p = 2.763$ Å and $q = 2.765$ Å, are in tetrahedral coordination. Each oxygen has four bonds in the first coordination sphere (cf. Table 2). Whereas the *q* bonds of each oxygen are symmetrically related, the *p* bond is symmetrically distinct.

The PBCs and primary surfaces having the surface structure of Figure 1 are derived graph-theoretically by program FFACE.[16]

Table 2. Strong Bonds between Water Molecules (Oxygen Atoms) in the First Coordination Sphere[a]

O1−O4	p	O3−O2 [0 0 −1]	p
O1−O3	q	O3−O1	q
O1−O3 [0 1 0]	q	O3−O1 [1 0 0]	q
O1−O3 [−1 0 0]	q	O3−O1 [0 −1 0]	q
O2−O3 [0 0 1]	p	O4−O1	p
O2−O4	q	O4−O2	q
O2−O4 [1 0 0]	q	O4−O2 [0 1 0]	q
O2−O4 [0−1 0]	q	O4−O2 [−1 0 0]	q

[a] Nonzero cell indices are shown in brackets.

Table 3. Chain Directions [*uvw*][16] and Face Indices (*hkl*) Satisfying "Flatness" Constructed from the Chain Directions[a]

primary form	(*hkl*)	[*uvw*]//(*hkl*)			
prism	(100)	[010]	[001]	[011]	[0 1 −1]
	(010)	[100]	[001]	[101]	[1 0 −1]
	(1 −1 0)	[001]	[110]	[111]	[1 1 −1]
pyramid	(101)	[010]	[1 0 −1]	[1 1 −1]	
	(1 0−1)	[010]	[101]	[111]	
	(011)	[100]	[0 1 −1]	[1 1 −1]	
	(0 1 −1)	[100]	[011]	[111]	
	(1 −1 1)	[1 0 −1]	[011]	[110]	
	(1 −1 −1)	[101]	[110]	[0 1 −1]	
basal face	(001)	[100]	[010]		

[a] Faces with symmetrically identical orientations are grouped together.

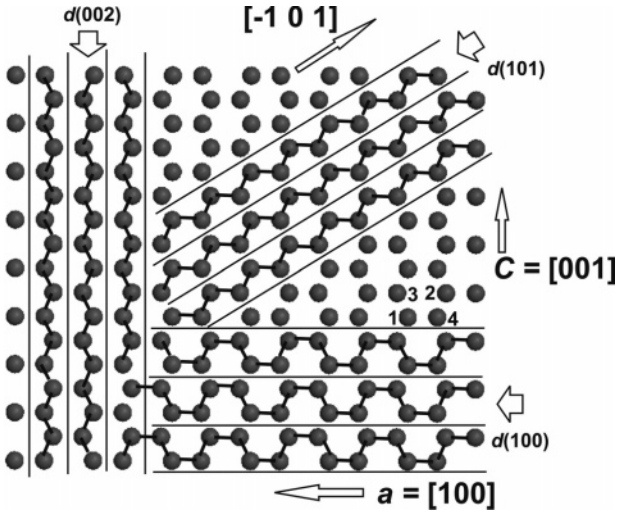

Figure 5. Three stacked growth layers of each primary surface, basal face d_{002}, prism d_{100}, and pyramid d_{101}, are shown edge-on in a projection perpendicular to the [010] direction. Straight thin lines indicate the slice boundaries of the molecular compositions. The oxygens of the unit cell are 1−4 and the lattice periods [100], [001], and [−1 0 1] are marked by arrows.

Table 3 lists in summary all the directions in which chains are found and the primary surfaces admissible by the flatness condition. For completeness, Figure 5 shows the orientations and molecular compositions[16] of the primary surfaces.

As can be seen from the list of PBC directions [*uvw*] in Table 3, pyramidal form (111) contains intersecting strong-bonding directions, yet it is neither a primary nor a secondary surface. Because no combination of the PBCs intersecting on the (111) plane can deliver a surface molecular composition satisfying the "flatness" condition, the molecular compositions belonging to the {111} family have the flatness-violating surface structure of Figure 2 and are unable to maintain well-defined unique surface orientations. {111} will likely not appear on the ice crystal growth form, or if it does, it should have a molecularly roughened appearance.

Several crystallographically important directions, having low-index lattice translations, contain no PBCs.[16] Examples: although PBCs exist in [011] and [0 1 −1], they are absent from the low-index directions [012], [0 1 −2], [021], and [0 2 −1]; although PBCs exist in [101] and [1 0 −1], they are absent from the low-index directions [102], [1 0 −2], [201], and [2 0 −1]; although PBCs exist in [110], they are absent from the low-index directions [1 −1 0], [120], [1 −2 0], [210], and [2 −1 0]. This leads to theoretically classifying some low-index crystallographic faces parallel to a single important PBC as secondary surfaces.

The important secondary surfaces, amenable to stabilization by external factors, have relatively large energy quantities, which amounts to relatively low crystallographic indices. They can be extracted from the list of infinitely many secondary surfaces, having the surface structure of Figure 3, as follows. The symmetrically distinct PBC directions are [001], [010], [1 0 −1], and [1 1 −1]. Of these, the first two are most important: [010] has the largest number of bonds per period, while [001] is found experimentally[43] to be a direction of growth promotion by the AFGP. Each PBC direction is parallel to infinitely many surfaces. Of those, the primary (flatness-observing and flatness-violating) surfaces are eliminated. Of the retained secondary surfaces, those with relatively low crystallographic indices are investigated further.

Faces parallel to the important PBC direction [001] are the prismatic forms {*hk*0}. The prism {100} resulting when $k = 0$ is here left out of consideration because it is a primary surface. Of the secondary prisms {*hk*0} with nonzero *h* and *k*, {110} and {120} have relatively low indices. (When $h = k = 2, 3, ...$, {*hh*0} is parallel to {110}.) Faces parallel to the important PBC direction [010] are the bipyramidal forms {*h*0*l*}. The pyramid {101} is here left out of consideration because it is a primary surface. Of the secondary pyramids {*h*0*l*} with *h* unequal to *l*, {102} and {201} have relatively low indices. (When $h = l = 2, 3, ...$, {*h*0*h*} is parallel to {101}.) The remaining secondary surfaces parallel to [001] and [010] have relatively high crystallographic indices. Thus secondary surfaces structurally capable of becoming kinetically stabilized are prisms (*hk*0), with nonzero *h* and *k*, such as (110), (120), up to, for example, (140), and pyramids (*h*0*l*) with nonzero and unequal *h* and *l*, such as (102), (201), (302), (203), up to, for example, (501).

4. Structural Ice Morphology

In this work the broken bond energies[46] are used as global indicators of the relative, that is, not the absolute, strengths of the various slice and attachment energies. They serve the purpose of comparison, in deciding whether the energy quantity of a given surface is smaller or larger than the corresponding energy quantity of another surface.

Slice and attachment energies in terms of bond strengths are tabulated in Table 4 for the primary surfaces and a selection of low-index (*hk*0) and (*h*0*l*) secondary surfaces.[14,18] The crystal energy is the sum of the slice and attachment energies, and it is a constant equal to $2p + 6q$, independently of the orientation (*hkl*). The energy quantities in the last two columns are normalized to $p = q = 1$.

In terms of normalized energies, the (100) prism and the (001) basal face (normalized growth rate 2 in Table 4) are of similar importance. Taking the central distances proportional to their

Table 4. Slice and Attachment Energies of the Primary and Some Secondary Surfaces[a]

face	E_{slice} (p, q)	E_{att} (p, q)	E_{slice} (norm)	E_{att} (norm)
	Primary Forms			
basal face (001)	$6q$	$2p$	6	2
prism (100)	$2p + 4q$	$2q$	6	2
pyramid (101)	$2p + 3q$	$3q$	5	3
	Secondary Forms			
prism (110)A,B,C	$2p + 2q$	$4q$	4	4
prism (120)A,B,C[b]	$2p + 2q$	$4q$	4	4
pyramid (102)	$p + 4q$	$p + 2q$	5	3
pyramid (201)	$p + 4q$	$p + 2q$	5	3

[a] Energies are expressed in terms of bonds, and in terms of bonds normalized to bond strength = 1, in order of decreasing slice energy. $E_{slice} + E_{att} = E_{crystal} = 2p + 6q =$ const. units per unit cell per mole. [b] The (210)A,B,C variants are equivalent to the (120)B,A,C variants, respectively, by symmetry.

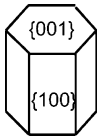

Figure 6. Structural ice morphology, that is, the morphology for which the structure is responsible in the absence of any external influence, based on attachment energies.

respective attachment energies[12−15] and taking into account geometrical factors, we can construct schematically (not to scale) the structural growth form of ice as shown in Figure 6. We find that the (101) primary pyramid (normalized growth rate 3 in Table 4) does not appear on the growth form because it happens to lie just below the threshold of appearance by a small amount. The threshold of appearance of (101) lies high for a geometric reason and because the attachment energy of (101) has the relatively large value of 3, as compared to the value of 2 for (001) or (100) (cf. Table 4). For that reason (001) and (100) dominate the morphology by suppressing (101). Should, however, some external factor cause a reduction in the growth rate of (101), bringing it below the theoretical level, then we may well observe the primary pyramid (101) on the growth form of ice.

5. Ice Morphology in the Presence of AFP

The most effective mechanism of enhancing preferentially some primary surfaces, of which the face indices are predetermined, is to occupy crystallographic sites and block parts of a surface. The approaching crystallizing units are delayed or prevented from reaching crystallographic sites and becoming incorporated in the crystal structure. Thus the strong binding of AFP molecules to the surface of ice will give rise to the pinning effect, which will hinder the movement of steps and inactivate the kinks at the surface. The two-dimensional insect type IBS possesses the necessary periodicity properties to match simultaneously the existing lattice translations in two intersecting directions.[7] But the variants of the fish-type IBS are not equipped for that task. Moreover, neither the "insect-type" IBS[7] nor the "fish-type" IBS variants (see below) offers a mechanism for transforming the flatness-violating molecular composition (111) from a molecularly roughened into a kinetically stable flat face.

A surface is considered to become "reconstructed" when dangling bonds on the surface combine to form additional (usually strong) bonds that are not present in the bulk structure. In this way, additional bonding enhances the surface involved by increasing its effective slice energy. Additional bonding can also take place in ways other than fusion of dangling bonds on the surface; there can also be AFP-induced additional bonding.

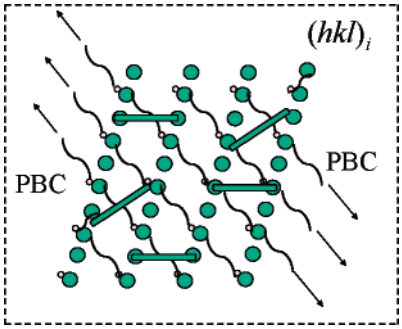

Figure 7. Schematic illustration of a statistical distribution of fish-type IBSs on a low-index secondary surface, inducing a surface-reconstruction type effect while selecting the face indices $(hkl)_i$.

The slice energies of the low-index (hk0) and (h0l) secondary surfaces in Table 4 are characterized by relatively high slice energies, comparable to those of the primary surfaces. For example, the slice energies of (110), (120), (102), and (201) are roughly $^2/_3$—$^5/_6$ the slice energy of the energetically strong primary prism (100). In terms of energy, the extra cost necessary to activate secondary surfaces such as (110), (120), (102), and (201) is not very high. The main impediment to the appearance of some secondary prismatic and pyramidal facets on the growth form of ice would not likely arise from a modest deficit in the energy of the surface bonding pattern. That impediment is rather due to the lack of bonding in a second lattice direction transverse to the single existing one.

To stabilize a secondary surface, the fish-type IBS introduces effectively a second strong-bonding direction to intersect with the existing one. This is schematically illustrated in Figure 7. Some of the surface molecular compositions available for engagement will offer a better match than others to the IBS structure. The selection of the face indices of the reconstructed surface occurs by identifying the particular surface molecular composition that offers the best structural match or the strongest interaction with a fish-type IBS. By providing supplementary bonding in various directions transverse to the existing strong-bonding direction, the IBS adjusts the surface orientation. Out of the numerous possibilities available for the surface orientations parallel to the PBC in Figure 3, the specific face indices $(hkl)_i$ are selected in Figure 7. Consequently, the indices of the observed ice facets are expected to vary according to the specific properties of the IBS of the AFP and according to the changes in the IBS caused by the experimental conditions.

The available experimental results show that the morphological modification mechanism of surface reconstruction is triggered by two variants of the fish-type IBS. The "one-dimensional" IBS variant found in fish type I AFPs and AFGPs is characterized by one or more linearly extended helices, having regularly spaced binding intervals in only one direction; cf. Figure 8a. It can align its helix/helices along any one of several alternative lattice translations transverse to the existing strong-bonding direction, thus mimicking a second intersecting strong-bonding direction that is absent from the crystal structure. The bridged distances are lattice periods between adjacent parallel (PBCs). So the one-dimensional IBS variant triggers surface reconstruction through "supplementary inter*chain* bonding". On

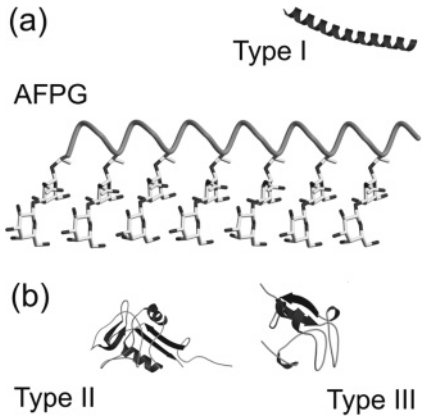

Figure 8. (a) One-dimensional helical variant of the "fish type" IBS: type I AFP (upper right) and AFGP (lower left). (b) Irregular globular variant of the "fish type" IBS having mixed α/β structure: type II AFP (left) and type III AFP (right).

the other hand, the "irregular" IBS variant found in globular type II and III AFPs, includes mixed α and β structures that are not one-dimensional. It need not be planar and its binding sites need not exhibit any spacing regularity in order to function; cf. Figure 8b. It can align itself along numerous shorter distances in various directions. It bridges intermolecular distances that need not be lattice translations, by linking oxygen−oxygen pairs on adjacent parallel PBCs. So the irregular IBS variant can trigger surface reconstruction through "supplementary inter*molecular* bonding".

6. Surface Reconstruction on Secondary Prisms

Secondary prisms (*hk*0), with nonzero *h* and *k*, containing the single strong-bonding direction [001], are usually observed in the presence of some fish AFPs and AFGPs:

(A) O1−*p*−O4−*q*−O2−*p*−O3[001]−*q*−O1[001]

(B) O1−*p*−O4−*q*−O2[−1 0 0]−*p*−O3[−1 0 1]−*q*−O1[001]

(C) O1−*p*−O4−*q*−O2[010]−*p*−O3[011]−*q*−O1[001]

Each PBC defines a growth block along (*hk*0) containing the full unit cell content. When the growth block is repeatedly translated along all lattice directions parallel to (*hk*0), the above PBCs generate three molecularly distinct growth layers $d_{hk0}{}^{A}$, $d_{hk0}{}^{B}$, and $d_{hk0}{}^{C}$. By way of illustration, only the PBCs A and B are considered below, generating the growth layers

$$d_{hk0}{}^{A} = \{O1, O2, O3, O4\}$$

and

$$d_{hk0}{}^{B} = \{O1, O2\,[-1\ 0\ 0], O3\,[-1\ 0\ 0], O4\}$$

The (110) and (120) surfaces serve to illustrate the process of surface reconstruction, as it might take place on any (*hk*0) prism. The lattice translations on (*hk*0) are in general [00*w*] but usually [001], and [−*k h w*] for arbitrary *w*. The [−*k h w*] directions are transverse to the single strong-bonding direction, [001], on (*hk*0). The lattice periods of [−*k h w*] are available for supplementary interchain bonding, by the one-dimensional

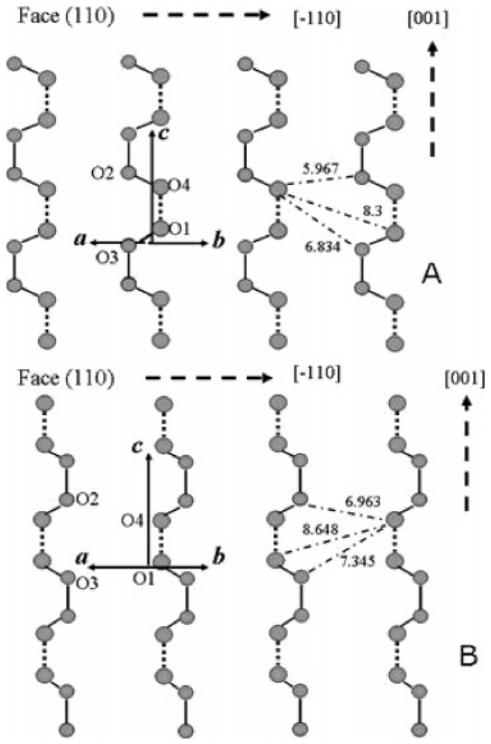

Figure 9. Distinct surface molecular compositions, $d_{110}{}^{A}$ obtained from PBC (A) in [001] (top) and $d_{110}{}^{B}$ obtained from PBC (B) (bottom), for a single growth layer. Larger circles denote oxygen atoms closer to the viewer; solid lines, O1−O3 and O2−O4 bonds; dashed lines, O1−O4 bonds; four adjacent PBCs are drawn; dashed arrows, PBC lattice period [001] = *c*-axis and transverse lattice period [−1 1 0] shown to scale define the plane of the paper (110). The single strong-bonding direction [001] supplemented by AFP-induced bonding along transverse directions [−1 1 *w*], for example, like [−1 1 0], causes surface reconstruction. The one-dimensional IBS variant is suited for interchain bonding along [−1 1 *w*] lattice periods. The irregular IBS variant is suited for intermolecular bonding of shorter distances, illustrated by dashed−dotted lines.

helical IBS variant. Other O−O distances to be described below, are available for supplementary intermolecular bonding by the irregular globular IBS variant. This enables the (*hk*0) surface to undergo reconstruction, whereby the specific (*hk*0) indices are selected so as to optimize the AFP−ice structural match or other interaction.

The growth layers $d_{110}{}^{A}$, $d_{120}{}^{A}$, $d_{110}{}^{B}$, and $d_{120}{}^{B}$ are depicted face-on in the structure projections of Figures 9 and 10, where PBCs A and B in [001] are discernible. Form {110} denotes the collection of symmetrically identical surfaces (110), (1 −2 0), and (2 −1 0) and their opposites (−1 −1 0), (−1 2 0), and (−2 1 0). The AFP interaction with the surface molecular composition of (2 −1 0), which is identical by symmetry to the surface molecular composition of (110) analyzed in this work, was the subject of scrutiny.[21]

The secondary prisms offer a rich variety of surface configurations for engagement by the IBS. The available molecular compositions abound not only due to the different surface orientations possible but also because alternative, symmetrically distinct, molecular compositions occur in each surface orientation. The probability for either IBS variant to attain the best structural match by engaging the most suitable surface molecular composition is high.

(21) Wierzbicki, A.; Taylor, M. S.; Knight, C. A.; Madura, J. D.; Harrington, J. P.; Sikes, C. S. *Biophys. J.* **1996**, *71*, 8−18.

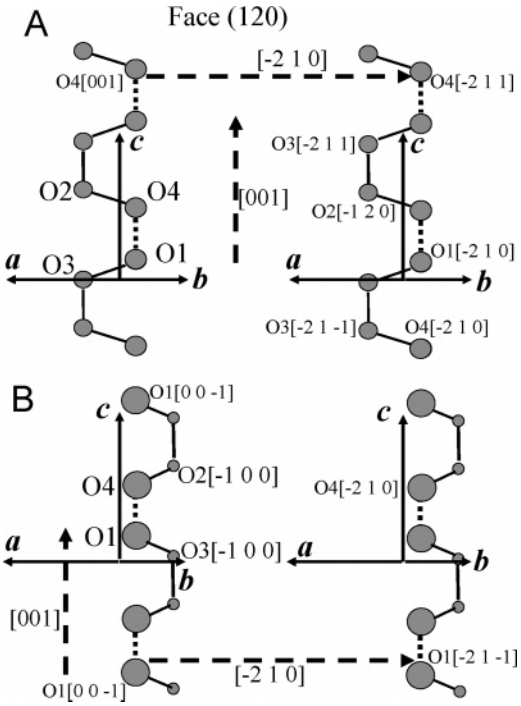

Figure 10. Distinct surface molecular compositions, $d_{120}{}^{A}$ obtained from PBC (A) in [001] (top) and $d_{120}{}^{B}$ obtained from PBC (B) (bottom), for a single growth layer. Symbols are as in Figure 9. Two adjacent PBCs are drawn. Transverse strong-bonding directions [−2 1 *w*], for example, [−2 1 0]. PBC lattice period [001] = *c*-axis and transverse lattice period [−2 1 0] shown to scale define the plane of the paper (120).

Table 5. Some Periods *L* of Transverse Lattice Translations [−*k h w*] Coplanar with (*hk*0) Available for Supplementary Interchain Bonding on Secondary Prisms (*hk*0)

(*hk*0)	[−*k h w*]	*L* (Å)
(110)	[1 −1 0]	7.827
	[1 −1 1]	10.742
	[1 −1 2]	16.667
(120)	[2 −1 0]	11.956
	[2 −1 1]	14.038
	[2 −1 2]	18.972
(140)	[4 −1 0]	20.710
	[4 −1 1]	21.976
	[4 −1 2]	25.404

The one-dimensional helical IBS variant could induce supplementary interchain bonding across parallel adjacent PBCs by bridging lattice translations transverse to [001]. Table 5 illustrates a selection of the lattice translations and lattice periods available to it for bridging parallel adjacent PBCs on the (110), (120), and (140) prisms. Some of the tabulated lattice periods are shown in Figure 9 on $d_{110}{}^{A}$ and $d_{110}{}^{B}$. The irregular globular IBS variant could induce supplementary intermolecular bonding across parallel adjacent PBCs by bridging shorter distances in various directions between oxygen pairs located on parallel adjacent PBCs. Table 6 illustrates a selection of the O−O distances available on the molecular compositions of the growth layers $d_{110}{}^{A}$ and $d_{110}{}^{B}$. Some of the tabulated O−O distances are shown in Figure 9 on $d_{110}{}^{A}$ and $d_{110}{}^{B}$.

In effect, both IBS variants can mimic one or more transverse coplanar PBCs that are absent from the structure, intersecting the original strong bonding direction [001]. The typical bridged distances involved in Tables 5 and 6 range from 6 to above 25 Å. So surface reconstruction through alignment on (*hk*0) is well within the capabilities of the fish-type IBS variants.

Table 6. Some O−O Distances between Adjacent Parallel Identical PBCs Transverse to [001] Available for Supplementary Intermolecular Bonding on Face (110) for the Molecular Compositions $d_{110}{}^{A}$ and $d_{110}{}^{B}$

O	O	distance (Å)
	$d_{110}{}^{A}$	
4	2 [−1 1 0]	5.967
4	3 [−1 1 0]	6.834
4	1 [−1 1 0]	8.3
3	2 [−1 1 0]	8.648
3	1 [−1 1 0]	10.746
3	4 [−1 1 0]	10.795
	$d_{110}{}^{B}$	
2 [−1 0 0]	4 [−1 1 0]	6.963
3 [−1 0 0]	4 [−1 1 0]	7.434
1	4 [−1 1 0]	8.648

7. Surface Reconstruction on Secondary Pyramids

Secondary pyramids (*h*0*l*), with unequal *h* and *l*, containing the single strong-bonding direction [010], are usually observed in the presence of the winter flounder AFP, often accompanied by loss of the symmetry on the plane perpendicular to the 6-fold axis.[22−24] The most widely documented face indices are (201).

Two PBCs in [010] contain half the unit cell content, consisting of two oxygen atoms each:

$$\text{(A) O1}-q-\text{O3[010]}-q-\text{O1[010]}$$

$$\text{(B) O2}-q-\text{O4}-q-\text{O2[010]}$$

The corresponding growth blocks are irrelevant, because they define two half-growth layers along (*h*0*l*), each containing half the unit cell content. After repeated translations parallel to (*h*0*l*), they would generate growth layers with half thickness, $d_{2h\,0\,2l} = (^1/_2)d_{h0l}$. Commonly half-layer growth is unlikely as it is not energetically favored. The above PBCs A and B can be linked by the strong bond O1−O4 and combined to form a third PBC C in [010], of which the molecular composition comprises the full unit cell content. After repeated translations parallel to (*h*0*l*), the corresponding growth block now contains growth layers with the full thickness d_{h0l}. Therefore a single molecular composition is possible, $d_{h0l}{}^{C}$, corresponding to PBC C:

$$\text{C} = \text{A} + \text{B} + (\text{O1}-\text{O4})$$

$$d_{h0l}{}^{C} = \{\text{O1, O2, O3, O4}\} = d_{h0l}$$

The lattice translations on (*h*0*l*) are in general [0 v 0] but usually [010], and [−*l* v *h*] for arbitrary v. The [−*l* v *h*] directions are transverse to the strong-bonding direction [010] on (*h*0*l*). The lattice periods of [−*l* v *h*] are available for supplementary interchain bonding, by the one-dimensional helical IBS variant. Other O−O distances, to be described below, are available for supplementary intermolecular bonding by the irregular globular IBS variant. This enables the (*h*0*l*) surface to undergo reconstruction, whereby the specific (*h*0*l*) indices are selected so as to optimize the AFP−substrate structural match or other interaction.

The molecular compositions of the (*h*0*l*) faces with the lowest crystallographic indices, (102) and (201), serve to illustrate the

(22) Harding, M. M.; Ward, L. G.; Haymet, A. D. J. *Eur. J. Biochem.* **1999**, *264*, 653−665.
(23) Fairley, K.;Westman, B. J.; Pham, L. H.; Haymet, A. D. J.; Harding, M. M.; Mackay, J. P. *J. Biol. Chem.* **2002**, *277*, 24073−24080.
(24) Houston, M. E. *J. Biol. Chem.* **1998**, *273*, 11714−11718.

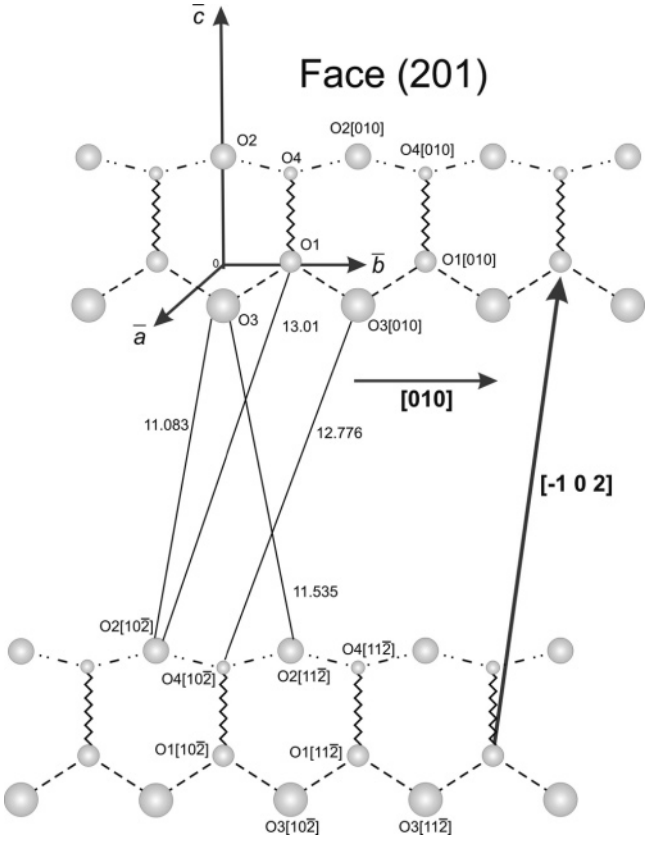

Figure 11. Surface molecular compositions d_{201} obtained from the composite PBC (C) in [010] for a single growth layer. Larger circles denote oxygen atoms closer to the viewer; dashed lines, O1−O3 bonds belonging to PBC (A); dashed−dotted lines, O2−O4 bonds belonging to PBC (B); wavy lines, O1−O4 bonds linking the two PBCs to form the composite PBC (C); only two adjacent PBCs are drawn; solid arrows, PBC lattice period [010] = *b*-axis and transverse lattice period [−1 0 2] shown to scale define the plane of the paper (201). The single strong-bonding direction [010] supplemented by AFP-induced bonding along transverse directions [−1 v 2], for example, [−1 0 2], causes surface reconstruction. One-dimensional IBSs are suited for interchain bonding along [−1 v 2] lattice periods; irregular IBSs are suited for intermolecular bonding of shorter distances, as illustrated by thin solid lines.

process of surface reconstruction, as it might take place on any (*h*0*l*) pyramid with molecular composition $d_{h0l} = d_{h0l}{}^{C}$. The composite PBC C in [010], together with its constituent PBCs A and B, and the surface molecular compositions d_{201} and d_{102} are shown in the structure projections on faces (102) and (201) in Figures11 and 12, respectively.

We see that multiple possibilities are available to the fish-type IBS for attaining the best structural match, by selecting the appropriate surface orientation. The one-dimensional helical IBS variant could induce supplementary interchain bonding across parallel adjacent PBCs by bridging lattice translations transverse to [010], thus mimicking a transverse PBC intersecting the original [010] PBC.

Table 7 illustrates some of the many possible lattice translations and periods available for supplementary interchain bonding on a range of (*h*0*l*) pyramids observed experimentally. The irregular globular IBS variant could induce supplementary intermolecular bonding across parallel adjacent PBCs by bridging shorter distances in various directions between oxygen pairs located on parallel adjacent PBCs. Table 8 illustrates a selection of the numerous O−O distances available on the molecular composition of the growth layer d_{201}. Figure 11 shows some

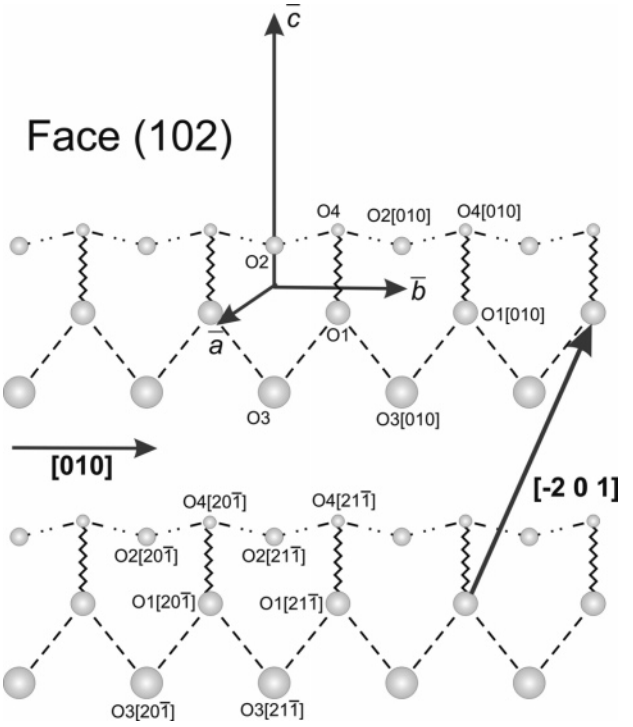

Figure 12. Surface molecular compositions d_{102} obtained from PBC (C) in [010] for a single growth layer. Symbols are as in Figure 11. Transverse strong-bonding directions [−2 v 1], for example, [−2 0 1]. PBC lattice period [010] = *b*-axis and transverse lattice period [−2 0 1] shown to scale define the plane of the paper (120).

Table 7. Some Periods *L* of Transverse Lattice Translations [*l v* −*h*], Coplanar with (*h*0*l*) and Available for Supplementary Interchain Bonding on Secondary Pyramids (*h*0*l*), Periods in Å

(*h*0*l*)	[*l v* −*h*]	*L* (Å)
(102)	[2 0 −1]	11.65
	[2 1 −1]	10.74
	[2 −1 −1]	14.04
(203)	[3 0 −2]	20.00
	[3 1 −2]	18.96
	[3 −1 −2]	21.95
(302)	[2 0 −3]	23.85
	[2 1 −3]	23.42
(201)	[1 0 −2]	15.39
	[1 2 −2]	16.66
	[1 −2 −2]	18.96
(301)	[1 0 −3]	22.53
	[1 2 −3]	23.42
(401)	[1 0 −4]	29.77
	[1 2 −4]	31.76

Table 8. Some Oxygen−Oxygen Distances between Adjacent Parallel Identical PBCs Transverse to [010], Available for Supplementary Intermolecular Bonding on Face (201), for the Surface Structure Generated by Molecular Composition d_{201}

O	O	distance (Å)
3	2 [1 0 −2]	11.083
3	4 [1 0 −2]	11.34
3	2 [1 1 −2]	11.535
1	4 [1 0 −2]	12.776
1	2 [1 0 −2]	13.01

oxygen−oxygen distances available for supplementary bonding in the surface molecular composition $d_{201}{}^{C}$.

Again, both IBS variants effectively can mimic one or more transverse PBCs that are absent from the structure, intersecting the original strong-bonding direction [010]. The typical distances

involved in Tables 7 and 8 range from 6 to above 30 Å and imply that surface reconstruction through alignment on (*h*0*l*) is well within the capabilities of the fish-type IBS variants.

8. Note on "Cut" Ice Pyramids: (201) and (111)

In Table 2 of ref 10, in simulating the AFP−ice−water system, use was made of face (201) as well as "a different cut" of face (201). On page 3 of ref 11, there appears a list of various ice planes used for docking of AFP type I. The first ice plane is (201), while the second ice plane is "(201) cut 2"! The so-called "different cut" or "cut 2" ice planes cannot be correct, since only one molecular composition exists in the (201) face that could grow as a stable flat face under the influence of an external factor.

As shown above, the kinetically less stable secondary surfaces (*hk*0) and (*h*0*l*) can be stabilized and activated as slowly growing surfaces. This is accomplished by means of surface reconstruction whereby the AFP distributes itself statistically throughout the surface and induces transverse bonding. In the [010] strong-bonding direction, only one PBC molecular composition of the full unit cell exists, PBC C, corresponding to only one growth layer d_{h0l}. Accordingly, in the specific case of (201), the single molecular composition is d_{201}. [This effect should be contrasted with the occurrence of three possible alternative molecular compositions, $d_{hk0}{}^{A}$, $d_{hk0}{}^{B}$, and $d_{hk0}{}^{C}$, of the full unit cell content, associated with the (*hk*0) prisms, and corresponding to three distinct [001] PBCs.] Therefore a "different cut (201)" or a "(201) cut 2" could only be a molecular composition not containing any PBCs whatsoever, and hence a kinetically highly unstable layer that is highly unlikely to become stabilized by an external factor.

Computer modeling of the IBS of a type II AFP was performed on the pyramidal (111) ice face in ref 25. It is not clear by which means (other than by an arbitrary cut) the employed molecular composition on (111) was determined and whether the inherent property of (111) to be molecularly roughened was considered. In concluding that "the fold of type II AFP could facilitate a stereospecific mode of interaction with (111) planes of ice",[25] the fact that (111) is neither crystallographically valid nor can it become stabilized kinetically by the AFP was overlooked.

These examples emphasize that performing simulations on substrates obtained by random cutting is meaningless.

9. Experimental Criteria for Testing Theoretical Predictions

Theoretical predictions concern the surface orientations featuring in the modified ice morphology; consequences of the interaction between fish-type IBS and engaged surface; and the relation between IBS, morphology and activity.

We saw that both fish-type IBS variants can align themselves along a multitude of lattice translations or oxygen−oxygen distances so as to trigger reconstruction of the engaged secondary surface. Alternative structure matches or other interactions between the ice substrates and the IBS are possible for various values of *h*, *k*, and *l* of the face indices (*hk*0) and (*h*0*l*). The closest structural match or optimal interaction selects the surface orientation and fixes the face indices.

Since the specific mode of interaction between secondary surface and IBS decides which surface should be engaged, we may expect to observe in experiment a variety of orientations of secondary prisms and pyramids. The dominant secondary surfaces may on occasion be combined with primary or other secondary surfaces. The molecularly roughened surface (111) is not expected to appear.

Theoretically, the stabilization of secondary surfaces by the fish-type IBS implies the alignment of that IBS along one or more directions transverse to the single strong-bonding direction. Moreover, the one-dimensional helical IBS should be aligned coplanar to the engaged surface. An exclusive alignment of any IBS along [001] on secondary prisms, or along [010] on secondary pyramids, could not lead to surface reconstruction and hence it is theoretically implausible. This holds for both methods of engagement: supplementary interchain bonding for the one-dimensional helical IBS variant or supplementary intermolecular bonding for the irregular globular IBS variant. For the secondary prisms, the IBS should be aligned on (*hk*0) along the [$-k$ h w] directions and not exclusively along the [001]. For the secondary pyramids, it should be aligned on (*h*0*l*) along the [l v $-h$] directions and not exclusively along the [010].

Symmetrically identical surfaces could well interact slightly differently with the IBSs distributed throughout the surfaces. It is theoretically possible that, in interacting differently with symmetrically identical molecular compositions, the IBS could cause a slightly different reduction in the growth rates of symmetrically identical facets, thereby introducing a decline in the outward symmetry of the crystallite.

Growth inhibition is attained by reduction of the growth rates of the crystal faces. A complete halt of the growth of ice would amount to the growth rates of all the ice growth fronts becoming zero. If the growth inhibition were successful for 100%, hardly any crystallites would be observed. In studying the resulting crystallites as modified by the AFP action, we are in effect working within a framework where the AFP-induced growth inhibition is incomplete, resulting in varying degrees of growth rate reduction. When the growth rates are reduced without actually dropping to zero, the various growth fronts experience a delay in their advance. The more severe the growth delay, the smaller the size of the resulting crystallites and the more successful the freezing inhibition. However, in the course of reducing all absolute growth rates, the AFP action may maintain the preexisting relations between the growth rates of the ice faces or it may allow these ratios to undergo modifications. In the former case the crystallite would look the same in the presence and in the absence of the AFP; only its absolute size would diminish. In the latter case, the resulting crystallites would have a different shape in addition to having a smaller size.

In the less successful AFP attempts, when the growth inhibition effect is marginal, the final crystallite size would not be very different from the original size, since the overall absolute values of the growth rates would not have decreased by much. Nevertheless the AFP action could well affect the relations between the growth rates without reducing their absolute values by a large amount. The resulting crystallites would retain close to their normal original size but may well exhibit a modified morphology.

Thus the AFP activity, that is, the degree of success of the AFP antifreeze action, is reflected in the overall size of the

(25) Wierzbicki, A.; Madura, J. D.; Salmon, C.; Sönnichsen, F. *J. Chem. Inf. Comput. Sci.* **1997**, *37*, 1006−1010.

resulting crystallite; that depends on the absolute growth rates. On the other hand, the mechanism by which the AFP acts is reflected in the morphological modification—or lack of modification—induced on that crystallite; that depends on the face indices and ratios between pairs of growth rates. A strong relation between IBS structure and morphology, as well as between IBS structure and activity, may be expected in experimental results. But no direct relation between morphology and activity need be observed.

In testing the theoretical prediction against experimental observation, the geometrical differences between prismatic and pyramidal faces become important. The prism is an open form, meaning that it cannot appear on the crystal habit by itself but only in combination with other forms, for example, basal plane and/or pyramid. A hexagonal prism seen in isolation cannot be distinguished from another differently oriented hexagonal prism. On the other hand, a hexagonal bipyramid is a closed form that can (and does) appear on the growth form by itself; however, it can also (and does) appear in combination with the basal face and/or various prisms. Bipyramids can readily be distinguished from other differently oriented bipyramids simply by visual inspection of the crystallite shape, which means the apical angle or the height-to-baseline ratio. For that reason, the broad range within which the experimentally observed pyramidal facets vary is directly observable on the obtained images published in the literature.

10. Comparison between Theory and Experiment

10.1. Variable Secondary Face Orientations and Combinations with Primary Surfaces. The secondary prismatic surfaces (*hk*0) contain the [001] direction. According to ref 43, the fish-type IBS enhances the growth rate along that direction. Their face indices, as observed in ref 26, vary from (110) up to (410). (110) is the most frequently reported secondary prismatic form. The identification of the (110) secondary prism in ice grown in the presence of sculpin AFP is reported in ref 26. According to refs 6 and 21, the sculpin AFP is responsible for the growth of prismatic (2 −1 0) ice crystals, where (2 −1 0) is symmetrically identical to (110). Combinations of secondary prisms with primary (and other secondary) forms are not ruled out theoretically. Indeed, ice crystallites grown out of a solution with AFGPs exhibit (*hk*0) surfaces,[28] sometimes in combination with the primary surface (100).[27]

The variation of secondary face orientations is more easily observed in the case of bipyramids. The secondary pyramidal surfaces (*h*0*l*) contain the most strongly bonded PBC, that is, the PBC in [010]. A large variety in secondary pyramidal shapes, as seen by height-to-baseline ratios or apical angles, has been observed, cf. Figures 13 and 14. Table 9 lists the estimated pyramidal face indices that best match a brief selection of the images published in the literature after a visual inspection of Figure 13. Figure 14 shows an assortment of images of ice pyramids obtained experimentally from AFPs with fish-type IBSs. The experimentally observed variety of secondary pyramidal surfaces activated by the fish-type IBS ranges from (302)

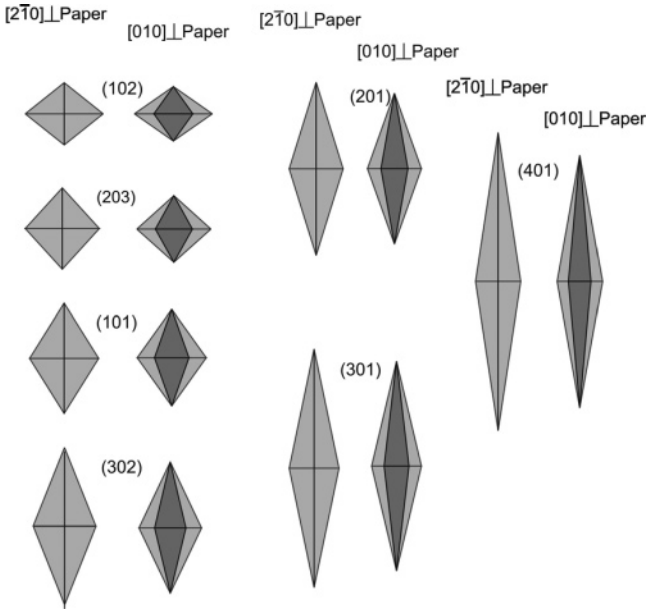

Figure 13. Outlines of ice pyramidal faces (*h*0*l*) encountered in a broad range of pyramid-shaped ice crystallites under the influence of (mostly) fish AFPs (absolute size is not to scale). [The ice pyramid face labeled (101) resembles those triggered by the insect TmAFP.]

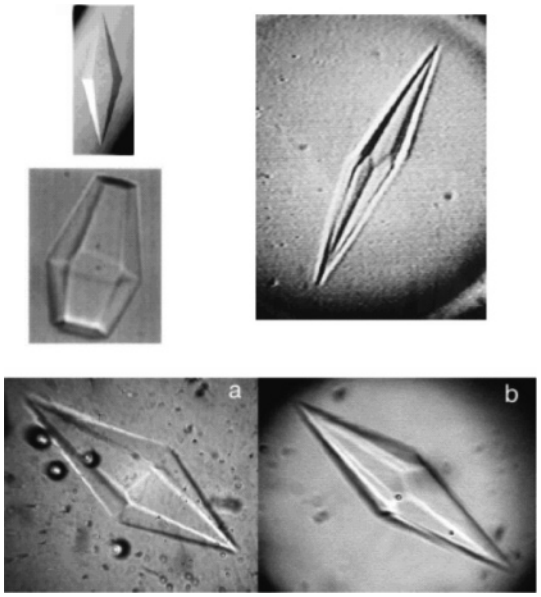

Figure 14. Experimental images of pyramids triggered by AFPs with fish-type IBSs. Top left: type I indexed as (201) (Figure 7A of ref 30; cf. also ref 31). Reprinted with permission from ref 30. Copyright 2003 American Chemical Society. Middle left: pyramid resembling (201) with reduced symmetry and in combination with basal face and possibly prism (Figure 4 of ref 24). Reprinted with permission from ref 24. Copyright 1998 Williams & Wilkins. Bottom (Figure 6 of ref 23): pyramids with clear reduction in symmetry, resembling (a) (201) and (b) (301). Reprinted with permission from ref 23. Copyright 2002 Williams & Wilkins. Top right (Figure 5 of ref 32): pyramid with higher index than (401), with further loss of symmetry. Reprinted with permission from ref 32. Copyright 1999 Federation of European Biochemical Societies.

to higher than (401). (201) is the most common secondary pyramid, triggered, among others, by the winter flounder AFP type I[22,29] and by the wild-type sculpin AFP.[23] According to

(26) Baardsnes, J.; Jelokhani-Niaraki, M.; Kondejewski, L. H.; Kuiper, M. J.; Kay, C. M.; Hodges, R. S.; Davies, P. L. *Protein Sci.* **2001**, *10*, 2566−2576.
(27) Wilson, P. W.; Gould, M.; DeVries, A. L. *Cryobiology* **2002**, *44*, 240−250.
(28) Harding, M. M.; Anderberg, P. I.; Haymet, A. D. J. *Eur. J. Biochem.* **2003**, *270*, 1381−1392.
(29) Haymet, A. D. J.; Ward, L. G.; Harding, M. M.; Knight, C. A. *FEBS Lett.* **1998**, *430*, 301−306.
(30) Walthen, B.; Kuiper, M.; Walker, V.; Jia, Z. *J. Am. Chem. Soc.* **2003**, *125*, 729−737.

Table 9. Comparison of Bipyramidal Ice Crystallites of Varying Face Indices Obtained in the Presence of AFP Mutants with the Pyramidal Forms (*h*0*l*) Drawn in Figure 13

reference	mutant	morphology
33, Figure 4	wild type	(302)
	L19A	(302)
	V20A	(201)
	V41A	(201)
	L10A/I13A	(301)
	L19A/V41A	(301)
34, Figure 2	BBB2KE[a]	(301)
	IIII2KE	(001) platelet
	TTTTAL2KE	(001) and (*hk*0)
	VVVVAL2KE	(001) roughened
32, Figure 5	LKAAK-A[a]	(401)
	LKAAK-B[a]	(401)
	AKAAK-C[b]	(401)
	AKAAK-D[b]	(401)
32, Figure 4	A17L(001)[a]	(201)
	A19L	(201)
	A20L	(201)
	A21L	(201)
29, Figure 2	VVVV2KE	(201)

[a] Loss of mirror normal to *c*-axis. [b] Loss of mirror normal to *c*-axis and 2-fold axis parallel to *c*-axis.

ref 23, no explanation for the specific occurrence of (201) has been given thus far. In line with the theoretical formulation, none of the pyramids produced by the fish-type IBS, as observed in Figure 14 or tabulated in Table 9, matches in shape the primary pyramid (101) drawn in Figure 13.

As expected, secondary pyramids appear in combination with primary (and other secondary) forms; the bipyramidal crystals depicted in the images of ref 24 are combined with the basal face (001) and also some unidentified prismatic facets. The theoretically admissible occurrence of combinations of secondary and primary surfaces can be verified in the experimental images. For example, a combination of (201) and (001) is observable in Figure 14a.

10.2. Experimental Absence of the (111) Bipyramid. In the ice structure the (111) bipyramid is unique in being the only kinetically unstable (i.e., flatness-violating) surface containing intersecting strong-bonding directions. The known IBS properties do not offer any plausible mechanism for stabilizing (111). It is predicted theoretically that (111) will be absent from the growth form of the ice crystals, or if it does appear, it should have a molecularly roughened appearance. Experimentally (111) is not observed on the usual ice morphology, and neither is there any experimental evidence for the occurrence of (111) on ice crystallites triggered by any AFP. Thus the experimental absence of (111) from the morphology agrees with the present prediction. However, that experimental result disagrees with the prediction of a computer simulation[25] carried out on an arbitrarily defined (111) surface cut.

10.3. Transverse Alignment of the IBS. Reference 21 reports that, in engaging one of the molecular compositions of the (2 −1 0) ice prism, which is symmetrically identical to the (110) prism (cf. Figure 9), the sculpin AFP aligns its helix along the [122] lattice translation. Alignment directions [*k h w*] like [122] or [−1 −2 2] are transverse to the only occurring PBC direction [001] and coplanar on the secondary prism (*hk*0) = (2 −1 0). As expected, the IBS is experimentally observed not aligned along the PBC direction [001], since an alignment along [001] could not bring about reconstruction of the (2 −1 0) surface.

After carrying out docking simulations of the fish type I AFP with energy minimization, Baardsnes et al.[35] concluded that, in binding on the (201) face, the IBS aligned itself along a direction equivalent to [1 0 −2]. The alignment direction [1 0 −2] was deduced from the surface-to-surface complimentarity observed in that work.[35] Yang et al.[41] also identified [1 0 −2] as the direction of alignment of the α-helix of the winter flounder type I AFP. The same observation had been made earlier by Wen and Laursen[36] while concluding that the fish AFP is unable to bind to the basal face.

Also, ref 21 reached the conclusion that the IBS is aligned along the zone ⟨012⟩ (a collective notation for symmetrically identical directions, one of them being direction [1 0 −2]). Thus the direction of alignment of the IBS on the secondary pyramid (*h*0*l*) = (201) is [−*l* *v* *h*] = [1 0 −2]; it is transverse to the single strong-bonding lattice direction [010] and coplanar on (201). Also in this case, the IBS is experimentally not aligned along the PBC direction [010], since an alignment along [010] could not bring about reconstruction of the (201) surface. The length of the binding interval of the fish type I AFP is not reported in ref 35, but the helix of the winter flounder AFP (wfAFP) is found experimentally to have a binding interval equal to $L = 16.5$ Å.[37] This is in good agreement with the values of 15.39 Å, equal to the lattice period of [−1 0 2], and of 16.66 Å, equal to the lattice period of [−1 −2 2] in Table 7.

10.4. Occasional Decline of Crystallite Symmetry. According to ref 21, the sculpin AFP aligns its helix on the (2 −1 0) ice prism along the [122] lattice translation but not along the symmetrically equivalent [−1 −2 2] lattice translation.[22] The adsorption of the IBS along a specific lattice direction, in preference to a symmetrically identical direction on the same face, is a natural consequence of the IBS helicity. No images of ice crystallites are provided by ref 22, but one would expect their growth forms to have a lower symmetry than prescribed by the space group.

In refs 23, 22, 32, 34, and 39, among other works, a decline in the symmetry properties of hexagonal ice is readily observable in the loss of the mirror plane normal to the 6-fold axis (the mirror plane is prescribed by the space group). This phenomenon has not yet been dealt with, so no explanation has been proposed. The loss of the mirror normal to the 6-fold axis observed in the pyramidal images of refs 23, 22, 32, 34, and 39, that is noticeable mostly in connection with high-index pyramids (cf. Figure 2 of ref 34 and Figure 5 of ref 32), is in agreement with the PBC theoretic analysis.

10.5. Predominant Dependence of Morphology on IBS Properties. Reference 23 reports that although AFPs of the sculpin and winter flounder families have closely related and

(31) Graether, S. P.; Kuiper, M. J.; Gagné, S. M.; Walker, V. K.; Jia, Z.; Sykes, B. D.; Davies, P. L. *Nature* **2000**, *406*, 325.
(32) Zhang, W.; Laursen, R. A. *FEBS Lett.* **1999**, *455* (3), 372.
(33) Baardsnes, J.; Davies, P. L. *Biochim. Biophys. Acta* **2002**, *1601*, 49−54.
(34) Haymet, A. D. J.; et al. *FEBS Lett.* **2001**, *491*, 285−288.
(35) Baardsnes, J.; Kondejewski, L. H.; Hodges, R. S.; Chao, H.; Kay, C. M.; Davies, P. L. *FEBS Lett.* **1999**, *463*, 87−91.
(36) Wen, D.; Laursen, R. A. *FEBS Lett.* **1993**, *317* (1, 2) 31−34.
(37) Knight, C. A.; Cheng, C. C.; DeVries, A. L. *Biophys. J.* **1991**, *59*, 409−418.
(38) Ewart, K. V.; Yang, D. S. C.; Ananthanarayanan, V. S.; Fletcher, G. L.; Hew, C. L. *J. Biol. Chem.* **1996**, *271*, 16627−16632.
(39) Nishimiya, Y.; Ohgiya, S.; Tsuda, S. *J. Biol. Chem.* **2003**, *278* (34), 32307−32312.

largely hydrophobic IBSs, the former engages secondary prisms such as (2 −1 0) while the latter engages the secondary pyramid (201). The explanation provided in ref 23 was that although both IBSs were indeed hydrophobic, they differed in their structure properties, such as the arrangement of their binding intervals. Reference 23 reports that although most sculpin AFPs produce prismatic ice crystals, some sculpin AFP variants and the wild type produce secondary pyramids with various degrees of activity. Here also, the root of the explanation could lie in the IBS structural aspects.

In the work of ref 38, the addition of divalent ions changes the IBS of the AFP so radically as to transform the crystal shape from secondary to primary facets and vice versa. Moreover, a recent experimental report on the action of dimer, trimer, and tetramer of type III AFP on ice crystals[39] states that each multimer "changes the morphology of a single ice crystal into a unique shape that is similar but not identical to the ordinary hexagonal bipyramid." The IBS of type III AFP belongs to the irregular globular IBS type. We notice in ref 39 that a substantial change in the IBS can cause a radical transition between pyramidal (Figure 2a of ref 39) and prismatic (Figure 2c of ref 39) forms, amounting to a strong, direct correlation between IBS structure and morphology.

10.6. Predominant Dependence of Activity and Crystallite Size on IBS Properties. The experimental results emphasize consistently an increase in AFP activity as the regularity of the intervals improves. Lin and Ewart[40] compared the skin-type and liver-type AFPs of the winter flounder. The skin-type showed a reduced activity as compared to the liver-type due to the lack of a complete ice binding motif. Zhang and Laursen[32] observed that a mutant of type I AFP with regular spacings showed antifreeze activity, whereas one with irregular spacings showed no activity. These results show the importance of the regularity of the binding intervals in the one-dimensional helical IBS variant, since in this case supplementary interchain bonding by bridging lattice periods is the mechanism by which surface reconstruction takes place.

According to a recent experimental report on type III AFP,[39] which has an irregular globular IBS variant, the thermal hysteresis increases in proportion with the size of the AFP, and hence of the IBS, reaching a maximum at lower concentration; this effect is accompanied by a drastic decrease in the size of ice with increasing concentration of the AFP.

10.7. Absence of Direct Correlation between Activity and Morphology. A morphological modification, as caused, for example, by surface reconstruction, implies a change in the *relative* growth rates but provides no information on the *absolute* growth rates. The drastic reduction in the absolute growth rates that is necessary for a successful attempt to inhibit freezing need not follow from the change in morphology. So a morphological modification per se does not imply a depression of the freezing point and may even accompanied by total protein inactivity; cf., e.g., refs 6, 24, and 35.

Baardsnes et al.[35] synthesized several mutants of AFP type I and measured the activity in relation to the activity of the wild-type wild protein. Those mutants that showed varied degrees of activity (including zero activity), measured as degrees of undercooling at different concentrations, gave rise to ice crystals with pure bipyramidal forms, cf. Figure 4 of that paper. As expected, no marked dependence of the shape of the bipyramid on the level of activity is observed; however, the size of the bipyramid decreases with increasing activity. The lack of any direct correlation between morphology and activity also follows from the more recent results of ref 39.

In agreement with the theoretical expectation, we see that the face indices (or pyramidal shape) do not depend on the AFP activity but both the shape and the AFP activity depend directly on the IBS characteristics. This experimental outcome does not support the belief that the morphological modification "inhibits further crystal growth".[42]

11. Discussion and Conclusions

The particular ice morphology observed under the AFP action is a direct consequence of the structural details relating to the adsorption mechanism of the AFP on the ice surfaces, so that different modes of adsorption trigger consistently and predictably different crystal habits. A correct PBC theoretic analysis of the growth processes, taking the AFP−ice system into account, led to the face indices, surface molecular compositions, and relative growth rates, as well as the mechanisms by which the various IBSs AFP induce morphological modifications. Primary, kinetically stable, slowly growing ice surfaces characterized by at least two intersecting strong-bonding directions and unambiguous face indices are associated with the action of the insect-type IBS.[7]

This work focused on the action of the fish-type IBS to reconstruct the secondary ice surfaces that are structurally capable of becoming kinetically stabilized by the AFP action. These are characterized theoretically by only one strong-bonding direction, implying that face indices are indeterminate. In the absence of the AFP action these kinetically less stable surfaces would not grow slowly with unique, well-defined orientations and hence would not appear in the morphology as flat surfaces. They become stabilized under the action of the fish-type IBS, which can induce preferentially transverse strong-bonding directions that are absent from the hexagonal ice structure. The one-dimensional helical variant can bridge transverse coplanar lattice periods. The irregular globular variant can bridge transverse shorter O−O distances that need not be coplanar.

The induced supplementary bridges crosswise on the engaged secondary surfaces decide specifically which of the possible surface orientations, with adjustable indices (*hk*0) and (*h*0*l*), will appear on the ice crystallite. The tendency of the AFP−substrate interaction to a maximum value serves to fix the orientation of the engaged surface. The observable crystallite shape has two structure-matching aspects: first, to induce an adequate surface bonding pattern necessary to mimic in effect the occurrence of a supplementary intersecting strong-bonding direction; and second, to maximize the IBS−ice structural match or other interaction. The two matching processes are interdependent; they occur not in succession but in unison. Experimentally the

(40) Lin, Q.; Ewart, K. V. *FEBS Lett.* **1999**, *453* (3), 331−334.
(41) Yang, D. S. C.; Hen, W.-C.; Bubanko, S.; Xue, Y. Q.; Seetharaman, J.; Hew, C. L.; Sicheri, F. *Biophys. J.* **1998**, *74*, 2142−2151.
(42) Madura, J. Fishy Proteins. In http://www.psc.edu/science/Madura/fishy_proteins.html.
(43) Yoshinori Furukawa, Hokkaido University, private communication.
(44) Graether, S. P.; Sykes, B. D. *Eur. J. Biochem.* **2004**, *271*, 3285−3296.
(45) Liou, Y.-C. *Nature* **2000**, *406*, 322−324.
(46) Sangwal, K.; Mielniczek-Brzoska, E.; Borc, J. *Cryst. Res. Technol.* **2003**, *38*, 103−112.

crystallites triggered by the fish-type IBS exhibit a large variety of secondary prismatic and especially pyramidal forms.

Since the AFPs are interspersed throughout the available surface, surface reconstruction has a statistical, as opposed to a structural, nature. Since, moreover, different structural matching schemes might well be not quite equally optimal, it is possible that some faces could be reconstructed differently from other, symmetrically identical facets, leading to a varying degree of growth rate reduction. This effect is experimentally observed as a decline or loss of some of the space group symmetry properties in the ensuing ice crystals.

The theory leads to a special dependence of the crystallite shape on experimental parameters. The indices of the observed ice facets are predicted to depend directly on the site-binding characteristics of the IBS of the AFP, with the understanding that experimental or other conditions can affect the structural characteristics of the IBS. The AFP activity as well as the crystallite shape are expected to depend directly on the detailed properties of the IBS. No direct correlation between the activity and the secondary prismatic and pyramidal face indices need be present. The AFP-induced modification of the ice morphology is the visible manifestation rather than the cause of the freezing inhibition.

The present PBC formulation provides a general and rigorous treatment applicable to any macromolecule with similar properties: that is, rigid IBSs with equivalent structures, and comparable distributions of hydrophobic and hydrophilic domains, as the AFPs. According to current knowledge, this combination of properties is unique to the AFPs. The available experimental evidence supports the theoretical findings, whereas no piece of experimental evidence has been found to contradict the theory.

Acknowledgment. We are indebted to Dr. Zhang Keqin and Dr. Li Dawei for assistance in preparing the figures and Mr. Jiang Huaidong for assistance with the submission of the manuscript.

JA047652Y